Synthesis and room-temperature NO_2 gas sensing properties of a WO_3 nanowires/porous silicon hybrid structure*

Zeng Peng(曾 鹏), Zhang Ping(张 平), Hu Ming(胡 明)†, Ma Shuang-Yun(马双云), and Yan Wen-Jun(闫文君)

School of Electronics and Information Engineering, Tianjin University, Tianjin 300072, *China*

(Received 29 August 2013; revised manuscript received 30 September 2013; published online 25 March 2014)

We report on the fabrication and performance of a room-temperature NO_2 gas sensor based on a WO_3 nanowires/porous silicon hybrid structure. The $W_{18}O_{49}$ nanowires are synthesized directly from a sputtered tungsten film on a porous silicon (PS) layer under heating in an argon atmosphere. After a carefully controlled annealing treatment, WO_3 nanowires are obtained on the PS layer without losing the morphology. The morphology, phase structure, and crystallinity of the nanowires are investigated by using field emission scanning electron microscopy (FESEM), X-ray diffractometer (XRD), and high-resolution transmission electron microscopy (HRTEM). Comparative gas sensing results indicate that the sensor based on the WO_3 nanowires exhibits a much higher sensitivity than that based on the PS and pure WO_3 nanowires in detecting NO_2 gas at room temperature. The mechanism of the WO_3 nanowires/PS hybrid structure in the NO_2 sensing is explained in detail.

Keywords: gas sensing, WO_3 nanowires, porous silicon, hybrid structure

PACS: 81.07.−b, 07.07.Df, 61.46.−w, 73.40.Lq **DOI:** 10.1088/1674-1056/23/5/058103

1. Introduction

The overwhelming progress of the human race in the last few decades has brought not only a technological revolution and comfortable living, but also unfortunate damage to the ecosystem by releasing more toxic gases into the environment. Nitrogen dioxide (NO_2), which results from combustions and automotive emissions, is one example. Furthermore, NO_2 is highly toxic to human nerves and respiratory organs, so highly sensitive detection to NO_2 gas is desired for monitoring air quality.[1–3] Gas sensors based on metal oxide semiconductors, including SnO_2,[4] WO_{3-x},[5] ZnO,[6] In_2O_3,[7] TiO_2,[8] and MoO_3,[9] have aroused a great interest of researchers in the recent years. The sensing mechanism is based on the change in electrical conductivity of metal oxides when gas molecules are adsorbed on the surface. Among extensive research for various metal oxide semiconductors, tungsten oxide (WO_3), which is a wide-band-gap n-type semiconductor, has been considered to be a promising material for NO_2 gas detection.[10–12] Actually, various tungsten oxide nanostructures (e.g., WO_3 nanowires,[13] nanorods,[14] and nanoplates[15]) have exhibited enhanced capabilities to detect NO_2 gas at low concentrations because of their large specific surface areas, monocrystalline structures and dimensions comparable to the Debye length. However, gas sensors based on tungsten oxide nanostructures usually work at a very high temperature (above 100 °C). Recently, porous silicon (PS) has been identified as a sensing material for room-temperature detection of NO_2 gas.[3,16] However, the sensing response was reported to be poor. Few efforts have been made to combine PS with WO_3 nanowires sensing element so that the properties of both materials could be efficiently exploited for the efficient detection of NO_2 gas, i.e., high response at a low operating temperature or at room temperature. Thus, in the present work, an effort is made to develop a novel gas sensor structure comprising of WO_3 nanowires loaded on PS to detect trace-level concentrations of NO_2 gas (0.1–2 ppm) at room temperature with enhanced sensing response characteristics.

2. Experimental section

Figure 1 illustrates the schematic diagram of the setup and a brief process for growing tungsten oxide nanowires. The PS layer was formed by electrochemical etching in a Teflon double-cell configuration which has been reported in our previous work.[17] In short, the specimen size was designed to be 22 mm × 8 mm after cutting from a p^+-type (100)-oriented monocrystalline silicon wafer with a resistivity of 0.001 Ω·cm. The specimen was cleaned and PS layers (the total area: 64 mm^2) were formed on the upper polished surface using the galvanostatic electrochemical etching method in 7.3 wt.% aqueous HF. A current density of 50 mA/cm^2 and an etching time of 20 min were used to prepare the PS layer. The etching process was carried out in the dark and at 25 ± 2 °C. Each PS sample was rinsed with ethanol and dried in air after anodization.

Prior to tungsten oxide nanowires growing on the PS substrate, a thin tungsten film was deposited on the PS substrate, first by DC facing target magnetron sputtering. The deposition was carried out under an argon (Ar) flow rate of 45 standard

*Project supported by the National Natural Science Foundation of China (Grant Nos. 61271070, 61274074, and 60771019) and the Key Research Program of Application Foundation and Advanced Technology of Tianjin, China (Grant No. 11JCZDJC15300).

†Corresponding author. E-mail: huming@tju.edu.cn

© 2014 Chinese Physical Society and IOP Publishing Ltd

cubic centimeters per minute (sccm), a DC power of 100 W and a pressure of 2 Pa at room temperature. After the sputtering, a 200 nm thick W film was obtained on PS substrate. Subsequently, the sputtered PS was placed in the middle of a quartz tube, which was mounted horizontally inside a tubular furnace. After the furnace was evacuated to a base pressure of 2 Pa, high-purity (99.999%) argon was introduced into the chamber at a constant rate of 35 sccm, and the chamber pressure was 150 Pa. The system was then heated to 700 °C for 1 h to induce the growth of tungsten oxide nanowires. After the furnace was cooled down to room temperature in the Ar ambient, the colorless W film was observed to change into a purple–blue film. The analysis showed that this film was not-fully-oxidized tungsten oxide, instead of the tungsten trioxide. For the preparation of WO_3 nanowires, the obtained sample was further annealed in air at 450 °C for 1 h.

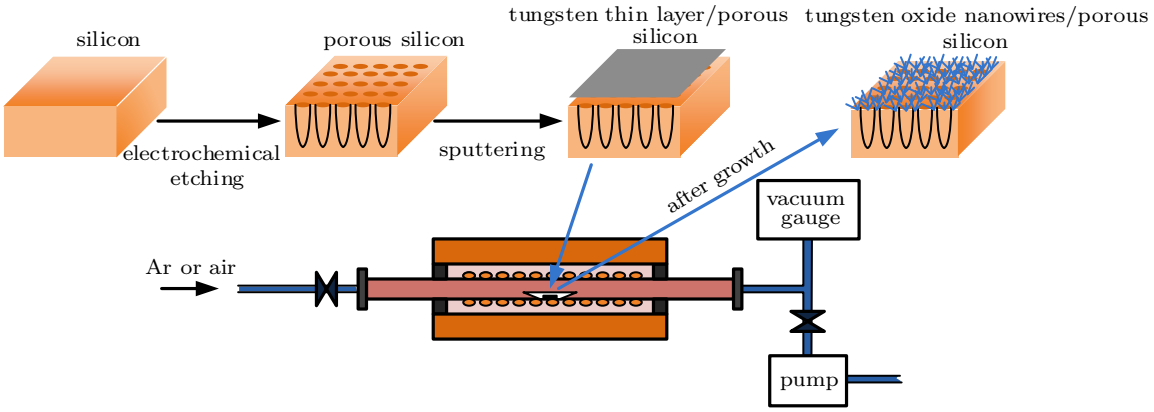


Fig. 1. (color online) Schematic diagram of the process and setup for growing tungsten oxide nanowires.

The prepared samples were analyzed first using the FEI Nanosem 430 field emission scanning electron microscopy (FESEM). Furthermore, the detailed one-dimensional (1D) nanostructures were characterized using X-ray diffractometer (XRD, RIGAKU D/MAX 2500 V/PC, Cu Kα radiation) and transmission electron microscopy (TEM, TECNAI G2 F20) at 200 kV for high resolution imaging.

For the fabrication of sensors, two electric contacts of a platinum (Pt) thin film with dimensions of 3 mm × 3 mm were deposited on the surface of WO_3 nanowires/PS by sputtering. The gas sensing characteristics were performed in a home-built static gas sensing testing system consisting of a test chamber, a flat heating plate, a professional digital multimeter and a data acquisition system, which was shown in Ref. [18]. Pure NO_2 gas was introduced directly into the chamber by a micro-injector to obtain a desired concentration. Changes in the resistance values of sensors during interaction with the target NO_2 gas were measured by the digital multimeter and sent to the computer. During data acquisition, humidity inside the test chamber was maintained at 30% RH at room temperature ($\sim$ 25 °C). The sensor response (S) to NO_2 was defined as $S = R_a/R_g$, where R_a and R_g are the resistances of the sensor element in the presence of atmospheric air and target gas respectively.

3. Results and discussion

3.1. Structure characterization

The morphologies of the PS layer and the one sputtered with tungsten thin film are investigated using FESEM. Figure 2(a) shows the typical surface morphology of the PS layer. The average pore diameter is approximately 22 nm, obtained by using an image analysis software (Nano Measurer 1.2). Moreover, the surface of the PS layer is etched completely, and the porosity of the PS layer is 64.3%. Porosity was determined by $P(\%) = (m_1 - m_2)/(m_1 - m_3)$[19] where $P(\%)$ is the porosity, m_1 is the sample weight before anodization, m_2 is the sample weight after anodization, and m_3 is the sample weight after removing the PS layer with a 1% KOH solution. Figure 2(b) presents the morphology of the tungsten film sputtered on the PS layer. The morphology drastically changes after the heat treatment in the Ar ambient. Figures 2(c) and 2(d) show different magnification SEM images of the tungsten oxide nanowires grown on the PS layer. High-density tungsten oxide nanowires cover the whole PS layer. The nanowires' lengths extend from 500 nm to 2 μm, and diameters range from 10 nm to 25 nm. The highest aspect ratio was estimated to be 200.

To identify the phase structure of the produced nanowires after the heat treatment in the Ar ambient, XRD, TEM, and high-resolution TEM (HRTEM) are performed. As shown in Fig. 3(a), the XRD patterns reveal that the main product could be a monoclinic WO_2 phase (JCPDS 32-1393). However, it should be noted that a sharp peak at around 23.5° is observed which can be indexed to a non-stoichiometric monoclinic $W_{18}O_{49}$ phase (JCPDS 84-1516), indicating the existence of nanowires on the sample. This result is consistent with the X-ray diffraction result of Koltypin *et al.*[20]

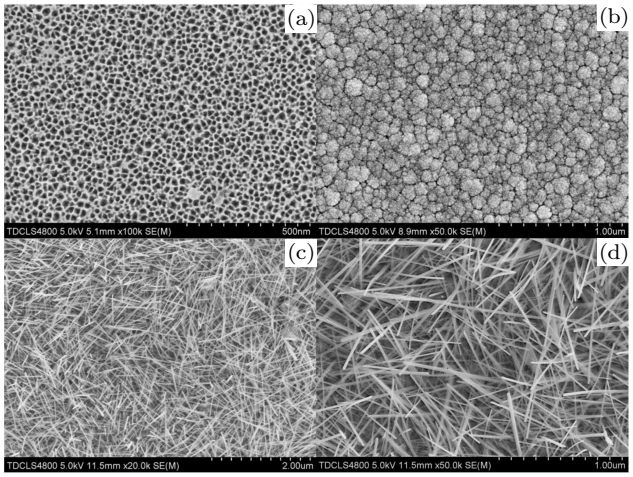


Fig. 2. SEM images of (a) pure PS and (b) PS sputtered with tungsten film. (c) Low magnification and (d) high magnification SEM image of produced tungsten oxide nanowires on PS after heating in Ar ambient.

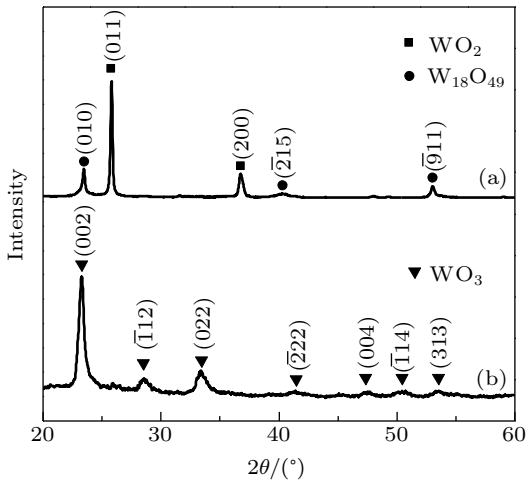


Fig. 3. XRD patterns of (a) the sample obtained by heating in Ar ambient, and (b) the sample obtained after annealing treatment in air at 450 °C for 1 h.

Figure 4(a) presents a low magnification TEM image of high-density tungsten oxide nanowires on PS, revealing the uniform growth of the nanowires. The high resolution TEM image of the nanowire future shown in Fig. 4(b) reveals visible planar defect features in parallel to the growth direction of the as-synthesized nanowires. The lattice fringe distance of 0.38 nm is consistent with the *d*-spacing of (010), and the fast Fourier transform (FFT) pattern is in conformity with the [001] zone axis of the monoclinic $W_{18}O_{49}$ phase (Fig. 4(c)). The growth direction of the nanowires is determined to be [010] of $W_{18}O_{49}$. The XRD peaks and TEM images indicate that WO_2 is formed in the initial stages of oxidation as the intermediate toward generation of the $W_{18}O_{49}$ nanowires. Due to the presence of the residual WO_2, which has a metal-like band structure at room temperature[21], a further annealing in air is required.

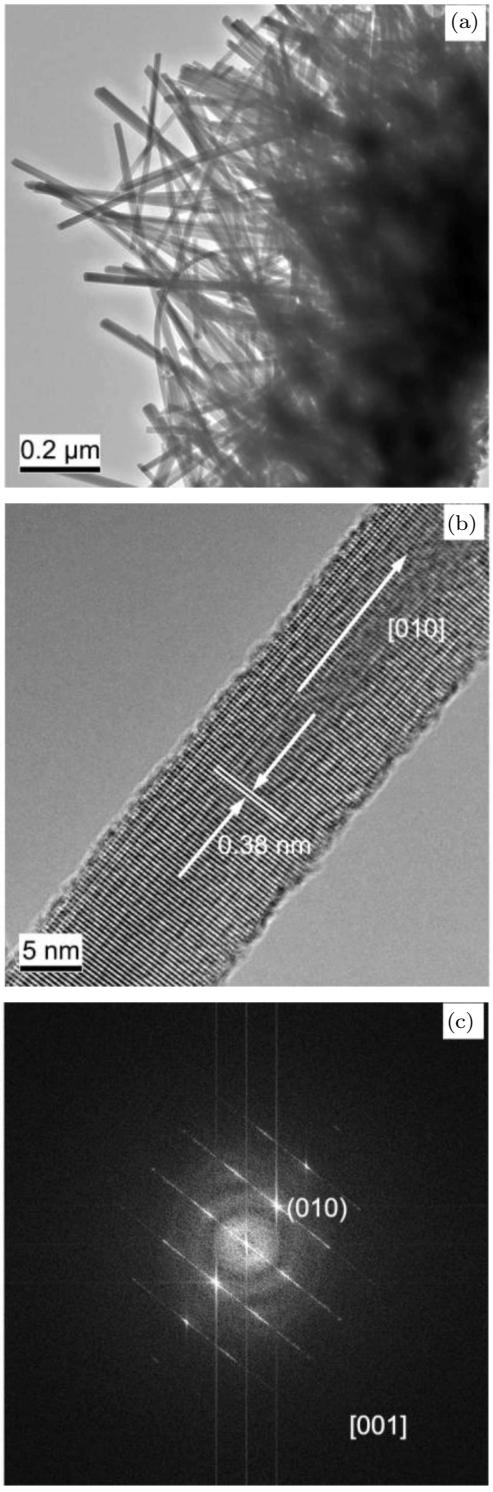


Fig. 4. (a) Low magnification and (b) high-resolution TEM image of $W_{18}O_{49}$ nanowires, and (c) fast Fourier transformation of the image (b).

Figure 5 shows the SEM images of the sample after annealing in air at 450 °C for 1 h. As shown in Fig. 5(a), the sample still keeps the nanostructure after annealing. However, the density decreases to some extent, which may be caused by the loss of tungsten species in the annealing process due to the generation of volatile tungsten species. Higher-resolution SEM images in Fig. 5(b) indicate that the nanowires have be-

come a bit curved and sharp, revealing the occurrence of deformation during the annealing treatment. XRD peaks in Fig. 3(b) can be assigned to monoclinic WO_3 phase structure (JSPDS 72-1465), indicating a phase transition of the sample after the annealing treatment.

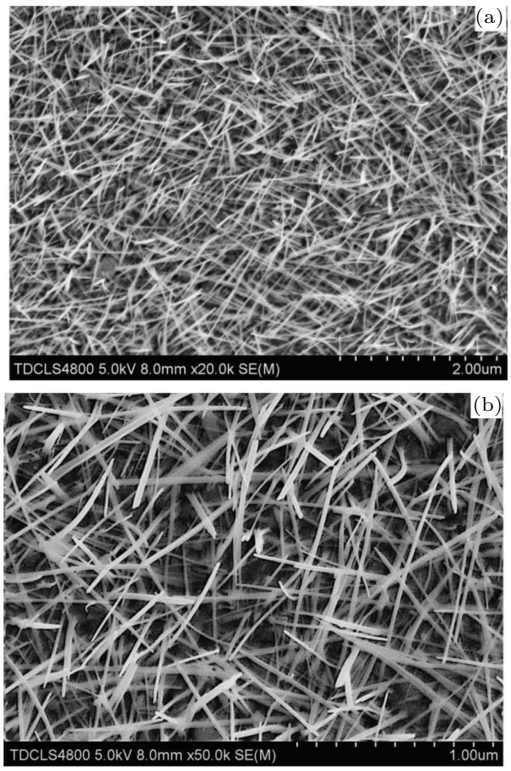


Fig. 5. (a) Low-magnification and (b) high-magnification SEM images of the sample after annealing treatment in air at 450 °C for 1 h.

The growth mechanism of the tungsten oxide nanowires restructured from tungsten film is suggested to be either the interface strain or the vapor–solid process, but the detailed mechanism is not well understood. According to the interface strain mechanism, the nanowires are grown by converting the strained oxide at the W/WO_x interface into the unstrained oxide in the nanowires.[22] In addition, Tokunaga *et al.*[23] observed that the initial growth of the nanowires did not consist of tungsten oxide but rather crystal tungsten. The crystal tungsten nanowires grown through cracks in the surface oxide layer on the tungsten film were then oxidized into tungsten oxide nanowires. Some authors assumed that the growth of nanowires is governed by the vapor–solid process since there is no catalyst involved in the growth.[24] The oxygen source for the growth of nanowires comes from the native oxide layer or the leakage of the system.

3.2. Gas sensing properties of NO_2

The gas sensing capabilities of different materials are investigated. In addition to the WO_3 nanowires/PS hybrid structure, sensors based on WO_3 nanowires/Al_2O_3 and pure PS are also fabricated and characterized. Figures 6(a) and 6(b) show typical response curves of a pure PS sensor and WO_3 nanowires/PS sensor respectively, measured at room temperature, for exposure to 500 ppb NO_2 gas. When the sensors are exposed to NO_2 gas, the resistances of both sensors decrease and soon afterward become saturated. After the removal of NO_2 gas, the resistances recover to their initial values. It is clear from the figure that the pure PS sensor is responsive to NO_2 gas at room temperature; however, resistances decrease further when WO_3 nanowires are loaded on the PS layer. WO_3 nanowires/Al_2O_3 do not show responsiveness to NO_2 gas (up to 2 ppm) at room temperature. This result is not surprising because, as is well known, pure WO_3 nanowires are not responsive to gas at room temperature. WO_3 nanowires/PS and pure PS both behave as p-type semiconductors, since their resistances decrease in the presence of oxidizing species. It should be noted that the recovery time of the sensor based on WO_3 nanowires/PS is longer than that of the pure PS sensor. This might be related to the high-density tungsten oxide nanowires or the oxide layer under the nanowires that remains without changing into nanowires; they block the passage of PS for gas desorption. The recovery process is found to be accelerated by heating the sensing materials at around 100 °C for a short duration (< 60 s) or by illuminating 365-nm-UV light for about 10 s. These phenomena are probably due to the activated

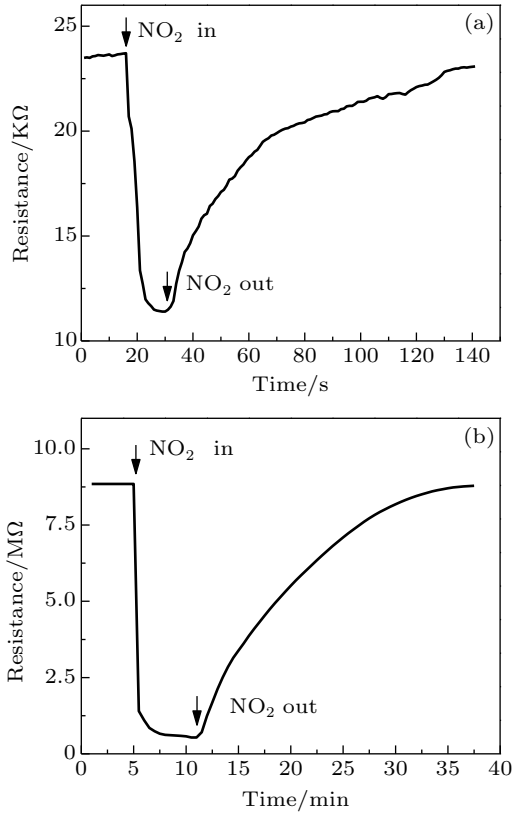


Fig. 6. Response and recovery characteristic to 500 ppb NO_2 gas at room temperature of (a) pure PS and (b) WO_3 nanowires/PS.

desorption process of adsorbent species by imparted thermal or photon energy as previously reported in other papers.[17,25]

Figure 7(a) shows the dynamic response curves of WO_3 nanowires/PS sensor upon exposure to NO_2 gas with different concentrations ranging from 0.1 to 2 ppm. We can see that as the gas concentration increases, the response is expanded. It can be seen that the sensor response increases obviously with the increase in NO_2 concentration, and the sensor is able to detect as low as 100 ppb of NO_2 gas with responsiveness near 4.28 when being operated at room temperature. This suggests that the sensor could monitor NO_2 gas in sub-ppm level at room temperature. Notably, the response value could not return to 1. In other words, the resistance value decreases marginally after NO_2 removal, indicating that a small number of NO_2 molecules fail to be desorbed from the surface, which might have a little influence on the gas sensing properties of the sensors. Figure 7(b) shows that the response magnitudes gradually increase as NO_2 concentration increases, for both pure PS sensor and WO_3 nanowires/PS sensors. It can be seen that the sensor responses greatly depend on NO_2 concentration, and the WO_3 nanowires/PS shows a higher response than the PS at various NO_2 concentrations. Clearly, the detection sensitivity defined by the slope of the response curve is found to be lower at high concentrations: roughly 31.4 per ppm in a range of 0.1–0.5 ppm, and 16.75 per ppm in a range of 0.5–2 ppm. Such a decrease in detection sensitivity at higher NO_2 concentrations might be explained by a partial saturation of the sensor at a high concentration.

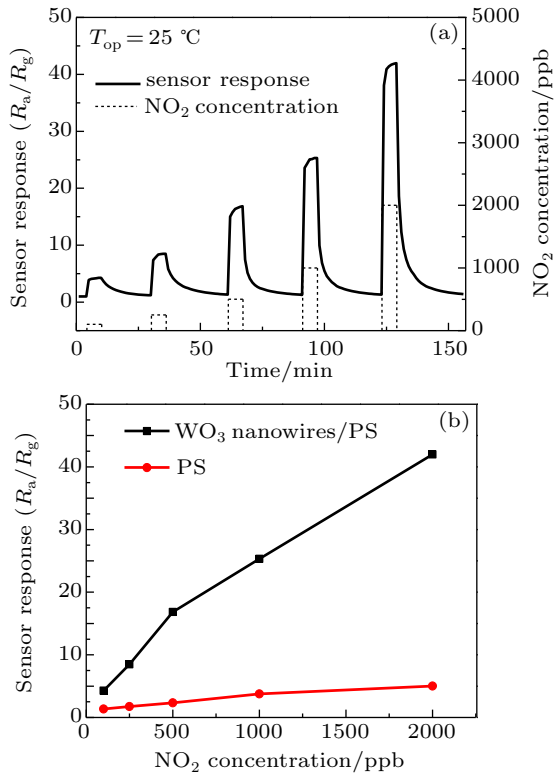


Fig. 7. (color online) (a) Dynamic response curve of WO_3 nanowires/PS versus concentration of NO_2 at room temperature. (b) NO_2 concentration dependent response values of pure PS and WO_3 nanowires/PS at room temperature.

3.3. NO_2 sensing mechanism

The mechanisms of the improved NO_2 sensitivity and the sensor gas-sensing behaviors are considered. As is well known, a higher surface-to-volume ratio for nanomaterials favors a larger number of surface oxygen vacancies. Hence the structural characteristics of the nanowires and PS result in a very large density of oxygen vacancy defects and dangling bonds, which makes the surface of the hybrid structure highly active to NO_2 gas. Besides, WO_3 is a well-known n-type semiconductor material and PS is a p-type semiconductor. This results in many heterojunctions at the interface of WO_3 nanowires and PS in the hybrid structure. A depletion layer is naturally formed at the interface between the p-type PS and the n-type WO_3 nanowire as shown in Fig. 8(a). Since WO_3 has a very low conductivity at room temperature, and thus a small density of electron carriers, the positive space charges in the WO_3 depletion region are distributed more sparsely than counterparts in the depletion region of PS. The difference in space charge density can develop a wide depletion layer towards the WO_3 nanowires and cause the band to bend upward. Furthermore, in the atmosphere, the oxygen molecules in the air will be absorbed onto the sensor surface and thus extract electrons from the conduction band of tungsten oxide and PS, and then transform into chemisorbed oxygen species (O_2^- and O^-) interacting with the target gas. The reaction kinematics may be explained by the following reactions:

$$O_2(\text{gas}) \rightarrow O_2(\text{ads}), \tag{1}$$

$$O_2(\text{ads}) + e^- \rightarrow O_2^-(\text{ads}), \tag{2}$$

$$O_2^-(\text{ads}) + e^- \rightarrow 2O^-(\text{ads}). \tag{3}$$

As a result, an electron-depleted space-charge layer is formed inside the oxide surface. The oxygen adsorption increases the depletion region, and the band bends further, thereby leading to the change of Fermi energy for oxides as shown in Fig. 8(b). The cooperation of heterojunctions and oxygen adsorption might induce the inversion. In the inversion layer, holes are indeed the major charge carriers, which indicates the p-type feature. Upon exposure to oxidizing NO_2, electron capture will significantly increase the hole concentrations of the inversion layer and PS, and simultaneously reduce the sensor resistance, that is,

$$NO_2(\text{gas}) + O_2^-(\text{ads}) + 2e^- \rightarrow NO_2^-(\text{ads}) + 2O^-(\text{ads}). \tag{4}$$

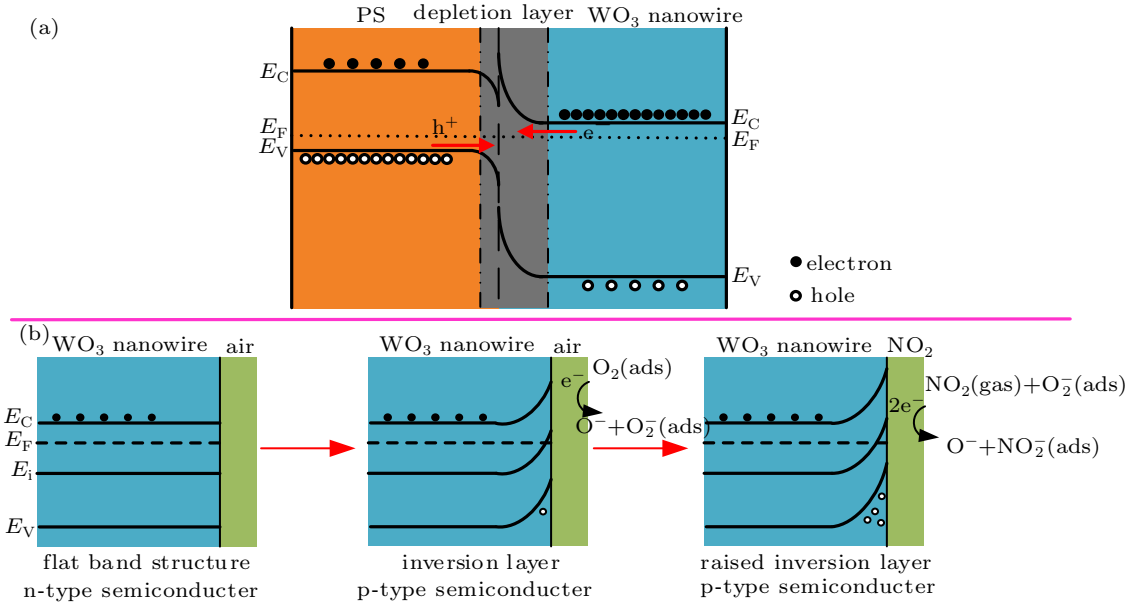


Fig. 8. (color online) (a) Proposed energy band structure diagram for WO_3 nanowires/PS heterojunctions in atmosphere. (b) Schematic energy-level diagram of WO_3 nanowire with absorption of oxygen and NO_2. E_C: lower level of conduction band, E_F: Fermi level, E_V: upper level of valance band, E_i: intrinsic level.

3.4. Selectivity

Gas sensors for practical applications are required to have not only a strong sensor response but also very good selectivity to target gases. It has been demonstrated that tungsten oxide sensors can be responsive to various gases, such as NO_2,[26] NH_3,[27] ethanol (C_2H_5OH),[28] O_3,[29] CO,[30] H_2[31], and H_2S.[32] Pure PS-based gas sensors have also been reported to have several applications in detecting NO_2,[33] NH_3,[34] H_2,[35] and various volatile organic compound gases such as ethanol, isopropyl alcohol, methanol, and acetone.[36,37] Therefore, it is necessary to perform research on the selectivity of WO_3 nanowires/PS. Figure 9 shows the response values of the sensor based on WO_3 nanowires/PS to 1 ppm NO_2, 20 ppm NH_3, 100 ppm isopropyl alcohol, 100 ppm ethanol, and 100 ppm methanol at room temperature. The sensor has a response to NH_3 to some degree, but the response value is only about 3.7, which is much less than its response value to NO_2 gas. In addition, there are no significant responses of the sensor to other three kinds of gases (S is less than 2). Therefore, WO_3 nanowires/PS has a very good selectivity to NO_2 gas.

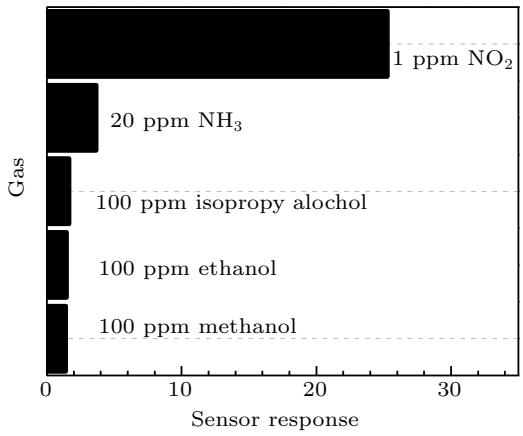


Fig. 9. Gas selectivity of WO_3 nanowires/PS to various gases.

4. Conclusions

High-density, monocrystalline $W_{18}O_{49}$ nanowires on PS are synthesized via a simple annealing treatment. The well-aligned nanowires exhibit uniform diameters, identical length values, and high density. The annealing treatment on the as-prepared sample can lead to the production of WO_3 nanowires without changing morphology. Compared with the pure WO_3 nanowire sensor and the pure PS sensor, the WO_3 nanowires/PS sensor exhibits a p-type semiconducting behavior with high sensitivity and good selectivity to different concentrations of NO_2 gas at room temperature. These results indicate the necessity of further studying the WO_3 nanowires/PS hybrid structure for NO_2 detection.

References

[1] Boarino L, Baratto C, Geobaldo F, Amato G, Comini E, Rossi A M, Faglia G, Lérondel G and Sberveglieri G 2000 *Mater. Sci. Eng. B* **69** 210
[2] Eranna G, Joshi B C, Runthala D P and Gupta R P 2004 *Crit. Rev. Solid State Mater. Sci.* **29** 111
[3] Rava M, Verlato G, Bono R, Ponzio M, Sartori S, Blengio G, Kuenzli N, Heinrich J, GötschiT and Marco R 2007 *Sci. Total Environ.* **384** 163
[4] Zhao Y, He X L, Li J P, Jia J and Gao X G 2012 *Chin. Phys. Lett.* **29** 070701
[5] Afzal A, Cioffi N, Sabbatini L and Torsi L 2012 *Sens. Actuat. B* **171** 25
[6] Xu L, Wang R, Liu Y and Dong L 2011 *Chin. Phys. Lett.* **28** 040701
[7] Belysheva T V, Bogovtseva L P, Kazachkov E A and Serebryakova N V 2003 *J. Anal. Chem.* **58** 583

[8] Kim I, Rothschild A, Lee B Y, Kim D Y, Jo S M and Tuller H L 2006 *Nano Lett.* **6** 2009
[9] Ganguly A and George R 2007 *Bull. Mater. Sci.* **30** 183
[10] Santucci S, Lozzi L, Maccallini E, Passacantando M, Ottaviano L and Cantalini C 2001 *J. Vac. Sci. Technol. A* **19** 1467
[11] Siciliano T, Tepore A, Micocci G, Serra A, Manno D and Filippo E 2008 *Sens. Actuat. B* **133** 321
[12] Liu Z F, Yamazaki T, Shen Y B, Kikuta T and Nakatani N 2007 *Sens. Actuat. B* **128** 173
[13] Deb B, Desai S, SumanasekeraG U and Sunkara M K 2007 *Nanotechnology* **18** 285501
[14] Ponzoni A, Russo V, Bailini A, Casari C S, Ferroni M, Bassi A L, Migliori A, Morandi V, Ortolani L, Sberveglieri G and Bottani C E 2011 *Sens. Actuat. B* **153** 340
[15] Hoa N D, Duy N V and Hieu N V 2013 *Mater. Res. Bull.* **48** 440
[16] Chen H Q, Hu M, Zeng J and Wang W D 2012 *Chin. Phys. B* **21** 058201
[17] Li M D, Hu M, Liu Q L, Ma S Y and Sun P 2013 *Appl. Surf. Sci.* **268** 188
[18] Qin Y X, Hu M and Zhang J 2010 *Sens. Actuat. B* **150** 339
[19] Sun P, Hu M, Li M D and Ma S Y 2012 *Acta Phys. Chim. Sin.* **28** 489
[20] Koltypin Y, Nikitenko S I and Gedanken A 2002 *J. Mater. Chem.* **12** 1107
[21] Shaposhnikov V L, Migas D B, Rodin V N and Borisenko V E 2011 *Phys. Stat. Sol.* **248** 1471
[22] Klinke C, Hannon J B, Gignac L, Reuter K and Avouris P 2005 *J. Phys. Chem. B* **109** 17787
[23] Tokunaga T, Kawanoto T, Tanoka K, Nakamura N, Hayashi Y, Sasaki K, Kuroda K and Yamamoto T 2012 *Nanoscale Res. Lett.* **7** 85
[24] Jeon S and Yong K 2008 *J. Mater. Res.* **23** 1320
[25] Law M, Kind H, Messer B, Kim F and Yang P D 2002 *Angew. Chem. Int. Ed.* **41** 2405
[26] Heidari E K, Zamani C, Marzbanrad E, Raissi B and Nazarpour S 2010 *Sens. Actuat. B* **146** 165
[27] Hieu N V, Quang V V, Hoa H D and Kim D 2011 *Curr. Appl. Phys.* **11** 657
[28] Su X T, Li Y N, Jian J K and Wang J D 2010 *Mater. Res. Bull.* **45** 1960
[29] Vallejos S, Khatko V, Aguir K, Ngo K A, Calderer J, Gràcia I, Cané C, Llobet E and Correig X 2007 *Sens. Actuat. B* **126** 573
[30] Park S, Kim H, Jin C, Choi S W, Kim S S and Lee C 2012 *Thermochim. Acta* **542** 69
[31] Hsu W C, Chan C C, PengC H and Chang C C 2007 *Thin Solid Film.* **516** 407
[32] Datta N, Ramgir N, Kaur M, Roy M, Bhatt R, Kailasaganapathi S, Debnath A K, Aswal D K and Gupta S K 2012 *Mater. Chem. Phys.* **134** 851
[33] Gaburro Z, Bettotti P, Saiani M, Pavesi L, Pancheri L, Oton C J and Capuj N 2004 *Appl. Phys. Lett.* **85** 555
[34] Seals L, Gole J L, Tse L A and Hesketh P J 2002 *J. Appl. Phys.* **91** 2519
[35] Ali N K, Hashim M R and Aziz A A 2008 *Solid State Electron.* **52** 1071
[36] Kim S J, Lee S H and Lee C J 2001 *J. Phys. D: Appl. Phys.* **34** 3505
[37] Salgado G G Becerril T D Santiesteban H J and Andrés E R 2006 *Opt. Mater.* **29** 51